HHS Public Access

Author manuscript

Connect Tissue Res. Author manuscript; available in PMC 2023 January 01.

Published in final edited form as:

Connect Tissue Res. 2022 January ; 63(1): 3–15. doi:10.1080/03008207.2020.1865938.

Effects of Raloxifene and tibial loading on bone mass and mechanics in male and female mice

Alycia G. Berman[1,¶], **John G. Damrath**[1,¶], **Jennifer Hatch**[2], **Alexis N. Pulliam**[2], **Katherine M. Powell**[2], **Madicyn Hinton**[2], **Joseph M. Wallace**[2,*]

[1]Weldon School of Biomedical Engineering, Purdue University, West Lafayette, IN, USA

[2]Department of Biomedical Engineering, Indiana University-Purdue University at Indianapolis, Indianapolis, IN, USA

Abstract

Raloxifene (RAL) is a selective estrogen receptor modulator (SERM) that has previously been shown to cause acellular benefits to bone tissue. Due to these improvements, RAL was combined with targeted tibial loading to assess if RAL treatment during periods of active bone formation would allow for further mechanical enhancements. To do so, structural, mechanical, and microstructural effects were assessed in bone from C57BL/6 mice that were treated with RAL (0.5 mg/kg), tibial loading, or both for 6 weeks, beginning at 10 weeks of age. *Ex vivo* microcomputed tomography (CT) images indicated RAL and loading work together to improve bone mass and architecture, especially within the cancellous region of males. Increases in cancellous bone volume fraction were heavily driven by increases in trabecular thickness, though there were some effects on trabecular spacing and number. In the cortical regions, RAL and loading both increased cross-sectional area, cortical area, and cortical thickness. Whole-bone mechanical testing primarily indicated effects of loading. Further characterization through Raman spectroscopy and nanoindentation showed load-based changes in mineralization and micromechanics, while both loading and RAL caused changes in the secondary collagen structure. In contrast to males, in females, there were large load-based effects in the cancellous and cortical regions, resulting in increased whole-bone mechanical properties. RAL had less of an effect on cancellous and cortical architecture, though some effects were still present. In conclusion, RAL and loading work together to impact bone architecture and mechanical integrity, leading to greater improvements than either treatment individually.

Keywords

Axial Compression; Computed Tomography; Mechanical; Strength; Raman Spectroscopy; Nanoindentation

[*]**Corresponding Author** Joseph M. Wallace, Ph.D., Department of Biomedical Engineering, Indiana University-Purdue University at Indianapolis, Indianapolis, IN, USA, jmwalla@iupui.edu, +1-317-274-2448.

[¶]These authors contributed equally to this work.

Declarations of Interests: None

1. Introduction

Raloxifene (RAL) is an FDA-approved selective estrogen receptor modulator (SERM) used to reduce fracture risk in post-menopausal women. It is a nonsteroidal benzothiophene that causes anti-resorptive effects in bone, which has been suggested *in vitro* to occur by both preventing osteoclastic and promoting osteoblastic activity [39]. These anti-resorptive effects occur without also stimulating proliferation of the breast and endometrium [15,22]. The efficacy of RAL in reducing vertebral fracture risk has been well demonstrated [16,36] and is comparable to that of bisphosphonates [12]. Despite this reduction in fracture risk, improvements in bone quantity due to RAL are modest, with a meta-analysis indicating that RAL increased bone mineral density (BMD) of the lumbar spine by only 2.5%, as compared to the 4.5–7.5% increase due to risedronate or alendronate [12]. Moreover, a logistic regression model indicated that changes in vertebral BMD only accounted for 4% of the measured reduction in fracture risk [34], suggesting additional non-mass based effects.

Although the exact mechanism by which RAL reduces fracture risk is unknown, pre-clinical studies have demonstrated that RAL improves material-level properties in bone independent of BMD [3–5]. Further *ex vivo* work has shown that, during mechanical loading, RAL alters the transfer of load between the collagen and hydroxyapatite, leading to reduced strains in the mineral and increased whole-bone toughness [20] and fatigue life [2]. These data suggest that RAL modifies the bone matrix independent of BMD, thus improving material-level properties of bone. For this reason, treatment with RAL during periods of active bone formation may allow for further mechanical enhancements due its potential ability to more readily access and thereby modify the collagen in the time period preceding mineralization.

One means of inducing active bone formation is mechanical stimulation. Clinically, this has been demonstrated through high-impact exercise such as running or jumping [11,13,19,46]. The exercise causes loading of the bone, which results in increased bone mass. *In vivo* non-invasive mechanical loading of the murine tibia has become a common means of loading bone [14,18,38,44,47]. In this model, the limb of the anesthetized animal is placed in a mechanical tester and cyclically loaded, causing a bone formation response. We have demonstrated a 15% increase in cortical thickness in mice that were loaded to 2050 με for two weeks [7].

Due to the mass-based improvements associated with loading and the material-level improvements associated with RAL, it was hypothesized that treatment with RAL during loading would improve bone mechanics beyond either treatment individually. In this study, this concept was tested in young male and female mice by treating them with RAL while simultaneously loading their right tibia. While tibial loading is not as clinically relevant as exercise, it often leads to larger mass-based gains [8]. Given that the primary goal of this study was to assess the effects of RAL during situations in which bone is being actively formed, tibial loading was utilized. For similar reasons, young mice were used due to their greater responsiveness to loading [45]. After treatment was completed, computed tomography and mechanical testing to failure were used to investigate changes in bone structure and function, respectively. In addition, material-level changes in the new bone tissue were assessed by Raman spectroscopy and nanoindentation.

2. Methods

2.1. Experimental Overview

Male and female C57BL/6 mice from an in-house colony were randomly separated into two groups: control (CON) and raloxifene (RAL). Beginning at 10 weeks of age, RAL mice were injected subcutaneously 5x/week with 0.5 mg/kg RAL. At the same time, both CON and RAL mice underwent compressive loading of the right tibia 3x/week. The contralateral limb served as a non-loaded control. Based on the sample sizes used in previous studies [7,23,25], one cohort (n=11–12/group/sex) was allocated to micro-computed tomography (micro-CT) and mechanical testing, while a second cohort (n=8/group; male only) was allocated to Raman spectroscopy and nanoindentation. Based on the results from cohort 1, only males were included in the second cohort so as to reduce the total number of mice. In this group, to enable detection of new bone growth for Raman spectroscopy and nanoindentation, the second cohort received a single subcutaneous calcein injection (0.15 mL) at the end of the first week. At 16 weeks of age, mice were euthanized by CO_2 asphyxiation and their tibiae were harvested and stored in phosphate-buffered saline (PBS)-soaked gauze at −20°C until use. Mouse numbers and groups are detailed in Table 1. These procedures and subsequent analyses were performed without blinding. All procedures were performed with prior approval from the Indiana University School of Medicine Institutional Animal Care and Use Committee (IACUC Protocol 11069).

2.2. In vivo Compressive Loading

Mice were anesthetized (2% Isoflurane) and their right tibiae were cyclically loaded in compression to a peak force of 10.6 N [7] for both males and females [27]. The loading profile consisted of 2 cycles at 4 Hz followed by a 1-second rest at 2 N, repeated 110 times for a total of 220 compressive cycles per loading day (3x/week).

2.3. Computed Tomography (CT)

The frozen, harvested tibiae were scanned by high resolution micro-CT (Skyscan 1172; Bruker, Kontich, Belgium) at a nominal isotropic resolution of 10 μm (V = 60 kV, I = 167 μA; 0.7-degree increment angle; 2 frame averaging). Hydroxyapatite calibration phantoms (0.25 and 0.75 g/cm3 CaHA) were used to convert gray-scale images to mineral content and to prevent day-to-day variation from becoming a potential confounding variable. After scanning, the tibiae were re-frozen at −20 C until mechanical testing.

The CT scans were then reconstructed (nRecon) and rotated (DataViewer) to enable consistent selection of the cancellous and cortical regions of interest. For cancellous analysis, a 1-mm thick region of interest in the proximal metaphysis was selected, beginning just distal to the growth plate and extending distally [32]. The cancellous bone was automatically segmented from the surrounding cortical shell in CTAn (Bruker) and then manually checked for accuracy. Each region of interest was then analyzed to determine bone volume fraction (BV/TV), trabecular thickness (Tb.Th), trabecular number (Tb.N), trabecular separation (Tb.Sp), bone mineral density (BMD), and tissue mineral density (TMD).

For cortical analysis, two 1-mm thick regions were selected. The first was centered at the mid-diaphysis (50% bone length) and the second at a proximal-mid location (37% of bone length) projected to be the site of highest tensile strain [8,37]. The mid-diaphysis was selected because it is the primary region that was mechanically tested, while the proximal-mid location was selected because it is the site of highest tensile strain and therefore, the chosen location for Raman spectroscopy and nanoindentation. A consistent grayscale threshold was used to segment bone from non-bone. These cortical regions of interest were analyzed in Matlab (MathWorks, Inc. Natick, MA) to determine areas (total cross sectional area, cortical area, and marrow area), cortical thickness, principal moments of inertia (maximum and minimum), and tissue mineral density [7,8].

2.4. Mechanical Testing

Following micro-CT, tibiae were monotonically tested to failure using four-point bending (3 mm inner loading span; 9 mm outer span) at a rate of 0.025 mm/sec. Tibiae were positioned with the loading fixture centered on the mid-diaphysis with the medial side in tension [7]. During testing, samples were kept hydrated by dripping PBS on the bone. From the load-displacement data, forces (yield and maximum), displacements (yield, post-yield, and total), work (yield, post-yield, and total), and stiffness were calculated. Load-displacement data were normalized to stress-strain using cortical mid-diaphyseal CT data in conjunction with standard four-point bending equations as described previously [7]. From the stress-strain data, stresses (yield and maximum), strains (yield, post-yield, and total), resilience, toughness, and elastic modulus were determined. To plot representative curves, the force-displacement and stress-strain values were averaged for each group at yield, maximum force, and failure locations.

2.5. Raman Spectroscopy

To prepare for Raman spectroscopy and nanoindentation, intact tibia from the second cohort were embedded vertically in individual glass tubes using a fast-curing methyl methacrylate (MMA) resin (Koldmount; SPI Supplies, West Chester, PA). After curing, embedded tibiae were carefully extracted from the glass tubes and mounted into a hydrated low-speed sectioning saw (IsoMet Low Speed Precision Cutter, Buehler, Lake Bluff, IL). Embedded tibiae were sectioned at 37% of the bone length measured from the proximal end [8], and polished using a 3 μm diamond suspension. After polishing, sections were rinsed with PBS and stored frozen in PBS-soaked gauze until use.

Raman spectroscopy was performed using an InVia Raman Spectrometer (Renishaw, Wotton-under-Edge, United Kingdom). A 785 nm laser was focused on the bone surface using a 50X objective to a spot size of ~1 μm. Using fluorescent calcein labels as guides, five regions of new bone spaced at least 10 μm apart in the posterior bone quadrant were assessed. For CON and RAL, new bone was assessed in the area inside the endocortical label while for LOAD and LOAD+RAL, new bone was assessed outside of the loading-induced periosteal label. The endocortical region was selected for CON and RAL samples because neither of these non-loaded groups exhibited periosteal calcein labelling as opposed to their loaded counterparts. Spectra were acquired following a 12s exposure at 5% laser power and were averaged across 10 accumulations. Baselines were corrected

using Renishaw WiRE intelligent fitting software, utilizing an 11th order polynomial fit, and cosmic rays were removed. Data was subsequently smoothed using a 2nd order Savitzky-Golay filter across 7 data points. Band intensities were calculated for v_1-PO_4^{3-} (959 cm^{-1}), v_1-CO_3^{2-} (1071 cm^{-1}), amide III (1246 cm^{-1}), CH_2 wag (1450 cm^{-1}), and amide I (1665 cm^{-1}) using GRAMS/AI (Thermo Fisher Scientific, Waltham, MA)Relative mineralization was determined by the mineral-to-matrix ratio, calculated as band intensity ratios of v_1-PO_4^{3-}/Amide I, v_1-PO_4^{3-}/CH_2 wag, and v_1-PO_4^{3-}/Amide III as previously described [24]. Mineral maturity/crystallinity was calculated as the inverse of the full width at half max of the v_1-PO_4^{3-} band. Type B carbonate substitution was calculated as the band intensity ratio of v_1-PO_4^{3-}/v_1-CO_3^{2-}. Relative collagen maturity was determined by fitting subpeaks within the amide I band via second derivative spectroscopy. 1660 cm^{-1} and 1690 cm^{-1} fitted beneath the amide I band. The spectral parameters calculated for each sample region were averaged, yielding a single value for each parameter for analysis.

2.6. Nanoindentation

Following Raman spectroscopy, samples underwent nanoindentation using a Hysitron TI 980 TriboIndenter (Bruker, Billerica, MA) equipped with a diamond Berkovich probe. Analysis was performed in the same regions of new bone as assessed by Raman spectroscopy. The loading profile consisted of a 30s loading period, a 120s hold at 1,000 μN, and a 30s unloading period. The resulting load-displacement curves were analyzed for reduced modulus and hardness as reported previously [31]. The data (N=5 per region) were averaged to produce a single value for each parameter per region.

2.7. Statistics

Data are presented as mean ± standard deviation, unless otherwise noted. In addition, each sex was statistically analyzed separately. Data were checked for normality of the residuals, and any violations were corrected with transformations. Extreme outliers (> 3*IQR) were removed. For CT and mechanical testing, a two-way repeated measures ANOVA was then used. Within this ANOVA model, the limb (right versus left) was considered the repeated measure and the treatment (RAL versus none) was considered the non-repeated measure. For Raman spectroscopy and nanoindentation, the two-way ANOVA was non-repeated due to the loss of some samples during processing. Main effects of treatment (between-subject effect), loading (within-subject effect), and their interaction ($p<0.05$) were analyzed. If the interaction term was significant, the two-way ANOVA was deemed invalid and instead, a one-way ANOVA was performed. If the one-way ANOVA was significant, a post-hoc Tukey's HSD test was used to assess differences between groups. All statistics were performed in Matlab (MathWorks, Inc. Natick, MA) using a custom script. In addition, Cohen's d was calculated for each group (loading, RAL, and combination) relative to the non-loaded control to assess relative effect sizes.

3. Results

3.1. Cancellous Bone Mass Show Improvements due to Loading and RAL in Male Mice and Primarily due to Loading in Female Mice

Loading and RAL both caused improvements to trabecular architecture in male and female mice (Fig 1A–B). In male mice, improvements to BMD and bone volume fraction were additive, with the combined treatment having greater effects than either treatment individually ($p<0.001$ for all comparisons; Fig 1C–D). Assessment of statistical effect size further demonstrate this additive response. For BMD, the statistical effect size was 1.00, 1.46, and 2.42 for loading, RAL, and the combined group, respectively, while for bone volume fraction, it was 1.13, 1.48, and 2.84, respectively. These improvements to bone volume fraction were driven, in part, by large increases in trabecular thickness ($p<0.001$ for loading and RAL; Fig 1E). While both loading and RAL improved trabecular thickness, only loading decreased trabecular separation ($p<0.01$; Fig 1F), and only RAL improved trabecular number ($p<0.01$; Fig 1G), suggesting differing mechanisms. Lastly, TMD was greater in the loaded mice ($p<0.01$; Fig 1H). A noteworthy observation was that, with the exception of trabecular thickness and TMD, the effect size due to RAL was larger than that due to loading. In addition, for all measurements, the combined effect size was greater than either loading or RAL individually.

Similar to the males, the females had positive effects due both loading and RAL. BMD and bone volume fraction were significantly improved by loading ($p<0.001$ for both), though RAL may also have had some effect on bone volume fraction given that the statistical effect size for the combination (2.64) was much larger than either that of loading (1.95) or RAL (1.07) individually ($p=0.06$; Fig 1C–D). In addition, both loading and RAL increased trabecular thickness, though the effects of loading were much greater (Fig 1E). Loading also reduced trabecular separation ($p=0.01$; Fig 1F) and increased trabecular number ($p=0.04$; Fig 1G). Although RAL did not have a significant impact on trabecular separation and number, the statistical effect sizes suggest that the combination treatment resulted in greater improvements than loading alone. Namely, for trabecular separation, the statistical effect size was −0.27 and −0.23 for loading and RAL, respectively, while in the combined group it was -0.62. Even more apparent, for trabecular number, the statistical effect size due to loading was only 0.28, while due to RAL was 0.68 and due to the combination was 0.88. Both loading and RAL influenced TMD (Fig 1H). For all properties except trabecular thickness and TMD, the combined effect size was larger than either loading or RAL individually.

3.2. Cortical Bone Mass in the Proximal-Mid and Mid Regions Show Effects of Loading and RAL in Males, but Primarily of Loading in Females

Similar to the cancellous region, the proximal-mid location showed additive effects of loading and RAL in the male mice, while in the female mice, the effects of loading were more pronounced than that of RAL (Fig 2A). In the male mice, total cross-sectional area, cortical area, and cortical thickness were improved by both loading ($p=0.02$, $p<0.01$, and $p<0.001$, respectively) and RAL ($p<0.001$ for all), with both treatments having similar effect sizes. When the treatments were combined, the gains were largest (Fig 2B–D). Loading

also significantly increased the maximum moment of inertia ($p<0.001$; Fig 2E), while both treatments increased the minimum moment of inertia ($p<0.001$ and $p<0.01$ for loading and RAL, respectively; Fig 2F). While TMD in the cancellous region was significantly impacted by loading, there was no effect in the proximal-mid location.

In the females, both loading and RAL had a significant impact on cross-sectional area and cortical thickness (Fig 2B, D). Loading also significantly increased cortical area ($p<0.001$; Fig 2C) and maximum moment of inertia (Fig 2E). Both loading and RAL significantly increased minimum moment of inertia (Fig 2F). TMD was also significantly increased with loading ($p<0.001$; Fig 2G).

As was shown for the cancellous and proximal-mid regions, within the mid-cortical region, loading and RAL had similar effects in the males, while in females, loading had a greater effect than RAL (Fig 3A). In males, cross-sectional area showed a graded response, only reaching significance in the combined treatment group (Fig 3B), whereas for cortical area and cortical thickness, the loading, RAL, and combined treatment were all significantly different from the non-loaded control (Fig 3C–D). Maximum moment of inertia showed similar trends as cross-sectional area, with results trending upward for loading and RAL but only reaching significance in the combined group (Fig 3E). For minimum moment of inertia, RAL had the greater effect (Fig 1F). For TMD, both RAL groups were significantly lower than the loaded control mice, but not the non-loaded control mice (Fig 3G).

For the female mice, cross-sectional area, cortical area, and cortical thickness were all improved with both loading and RAL (Fig 3B–D), while maximum and minimum moments of inertia were only impacted by loading (Fig 3E–F). There was no effect of either loading or RAL on TMD.

3.3. Mechanics Primarily Show an Effect of Loading in Both Males and Females

Four-point bending to failure, which primarily tests the mechanical integrity of the mid-cortical region, showed a similar response to loading and RAL as was observed by CT. Namely, in males, loading and RAL both improved the structural-level mechanics, though there was no additive effect of the combined treatment, while in females, loading alone drove the improvements (Fig 4A–C; Table 2). After normalizing to bone size, estimated material-level mechanics indicated significant improvements due only to loading in male and female mice (Fig 4D–F; Table 2). Although non-significant, total work and toughness both trended upward with the combined treatment in females. Analysis of effect size highlighted this observation in that Load, RAL, and RAL+Load had increasing effect sizes for total work (0.628, 0.709, and 0.865, respectively) and toughness (0.368, 0.651, and 0.665).

3.4. Loading and Raloxifene Treatment alter Matrix Composition in Newly Formed Bone

Regions of new bone growth were determined using fluorescent calcein labels (Fig 5A–D). For the loaded bones, the periosteal surface was assessed, while for the non-loaded bones, the endocortical surface was assessed due to the lack of periosteal labelling. Raman spectroscopic measures of relative mineralization, as described by both the $\nu 1\text{-}PO_4^3$/Amide I and $\nu 1\text{-}PO_4^3$/Amide III band intensity ratios, were not significantly impacted by loading

or RAL treatment. However, when calculated as the $\nu 1\text{-}PO_4^3/CH_2$ wag band intensity ratio, relative mineralization was significantly increased by loading ($p < 0.001$), but not RAL (Fig 5E). Similarly, mineral crystallinity was also significantly increased in loaded limbs ($p = 0.04$) but was not affected by RAL treatment (Fig 5F). Both loading and RAL did cause an increase in Type B carbonate substitution as determined by the $\nu_1\text{-}CO_3^{2-}/\ \nu_1\text{-}PO_4^3$ band intensity ratio ($p = 0.02$ and $p < 0.01$, respectively; Fig 5G). Finally, relative collagen maturity was significantly increased by both loading and RAL treatment (Fig 5H).

3.5 Loading Increases Reduced Modulus and Hardness in Newly Formed Bone

In an effort to understand the local mechanics of the newly formed bone, we calculated hardness and reduced elastic modulus from nanoindentation curves (Fig 6). Results showed that both were significantly increased in limbs that underwent loading ($p < 0.01$ and $p < 0.01$, respectively), but not significantly altered by RAL treatment.

4. Discussion

Raloxifene is a selective estrogen receptor modulator (SERM) that has been shown to reduce fracture risk in osteoporosis patients [10,20] through both quantity- and quality-based improvements. We therefore hypothesized that the presence of RAL during periods of active bone formation (i.e. prior and during mineralization) would enable tissue-based improvements to a greater degree than during periods of little bone formation. In addition, while previous work has demonstrated that adding aerobic exercise during RAL treatment can further increase BMD [51], little work has been performed to assess the individual and combined impacts of RAL and mechanical stimulation, especially as it relates to metrics beyond that of BMD. Results in males demonstrate that loading and RAL have distinct impacts on the bone tissue, making the combination treatment a consideration to provide additional improvements beyond either treatment alone.

Tibial loading is a common method used to induce a robust bone formation response [7,8,14,18,38,44,47]. While physical exercise, such as running, is more clinically relevant, tibial loading has the advantage of a more robust bone-formation response [8]. Previous work from our group has shown that loading female C57BL/6 mice to 10.6 N for only 2 weeks (9 total loading bouts) can increase cortical thickness by 15% [7]. In the current study, we extended the loading to 6 weeks to provide additional time to observe the effects of RAL, and noted an average mid-cortical thickness increase of 26% in females. For the males, we chose to use the same peak load level as for females (10.6 N), given previous work that showed similar adaptive response in the cancellous region for both sexes [27]. Our work, in general, showed less responsiveness in the males than females (although the comparison was not statistically analyzed). In the cortical region, this difference in responsiveness is demonstrated by the 12% increase in cortical thickness observed with loading in the CON males compared to the 26% increase observed in CON females. In the same way, in the cancellous region, loading resulted in a 22% increase in bone volume fraction in CON males, compared to the 58% increase in females. One potential reason for this discrepancy could be an increase in background activity (e.g. cage fighting) among the group-housed males [30]. Alternatively, there may have been differences in load level and profile; however, since we did not verify

strain levels induced in the bone prior to this study, direct comparisons are challenging. Even so, our primary objective in loading the tibiae was to induce a robust bone formation response which did occur in both males and females.

During this period of active bone formation, RAL was given to the mice. Previous work with RAL has demonstrated its ability to improve post-yield behavior in bone [20]. In addition, the mere presence of RAL *ex vivo* alters the transfer of load between the collagen and hydroxyapatite during mechanical loading [20]. Since the studies were shown in mineralized bone where access to the collagen may be inhibited, we hypothesized that RAL during tibial loading would create an environment whereby bone could be further improved. In this regard, we did observe some beneficial effects of RAL and loading, though the most pronounced effects were the mass-based outcomes observed within the cancellous region. In the clinic, RAL is known to only modestly improve bone mass, making these preclinical results interesting. Even so, these results do align with other preclinical work [32,33]. While cancellous effects were additive, effects in the mid-cortical region appeared to plateau. RAL and loading both had a positive impact, but their combination provided only modest further benefit.

RAL, like loading, improved maximum mechanical force. However, in the combination group, the effect plateaued such that loading, RAL, and the combination treatment all showed similar improvements. In females, the RAL+loading seemed to recover post-yield properties, increasing the effect size of total work and toughness versus non-loaded control bones, though results were non-significant. A previous study exploring the combination of RAL and a bisphosphonate treatment showed similar modest effects of RAL on mechanical properties [33]. Of particular interest is that, in that study, the effect of treatment on diseased bone was greater than that of healthy bone in the osteogenesis imperfecta murine model. While it is unclear why there were few whole-bone mechanical effects due to RAL in the current study, the previous work does suggest that bone may reach a point such that it is hard to make the already healthy bone any better [33]. As such, applying this combined treatment strategy in diseased bone is an important next step.

While whole-bone mechanical improvements were primarily loading-based, the secondary goal of this study was to assess if the newly deposited bone matrix was materially different among the treatment groups. For this sub-study, the decision to use only male mice was driven by a concern that the large loading-based effects in females would obscure the effects of RAL in the combined treatment group. In contrast, the mass-based effects in males at the proximal-mid location was graded, showing clear contributions of both loading and RAL. Others have reported that although bone size and shape are heavily affected by sex, the tissue-level material properties are less dependent [40]. For these reasons, we chose to focus the Raman spectroscopy and nanoindentation on male mice.

When normalizing phosphate peak intensity by that of the amide I or amide III bands, relative mineralization remained unchanged. However, since this metric is relative, it may be that the osteoblasts deposited both mineral and collagen, resulting in no change in the mineral-to-matrix ratio. This finding is further supported by the increased modulus and hardness in bone that underwent loading, which is most likely due to increased

local mineralization [1]. Like loading, RAL has been shown to increase osteoblast collagen deposition, as well as slightly increase or preserve bone mineral density [26], which may have similarly resulted in a zero net change in these mineral/matrix ratios. Interestingly, a significant effect of loading was found when comparing the phosphate peak intensity to that of the CH_2 wag peak. In bone, the CH_2 wag peak originates primarily from the side chains of glycine, proline, and hydroxyproline found in collagen [35]. It is therefore possible that mechanical loading led to increased non-collagenous proteins (NCPs) in the bone matrix that contribute to the amide peaks, but due to their smaller CH_2 content compared to collagen, contribute little to the CH_2 wag peak.

Loading also significantly increased mineral crystallinity which is interesting given the lack of effect on type B carbonate substitution. In synthetic HA, increasing carbonate substitution typically decreases crystal perfection as carbonate substitutes for phosphate, increasing the length of the *c*-axis while decreasing the *a*-axis [29,50]. However, it should be noted that crystallinity also assesses the size and shape of the mineral crystals and not just perfection, which may have driven these effects. In addition, while the inverse relationship between carbonate substitution and crystallinity has been observed in bone, several studies examining the effects of aging on matrix composition have noted that crystallinity and carbonate content each tend to increase with age [1,49]. While the change in crystallinity was modest, it is possible that loading induced additional changes in crystal substitution that normalized the overall crystallinity measure. Further studies are needed to assess the contribution of additional ionic substitutions to the Raman crystallinity parameter.

Although loading did not increase type B carbonate substitution, RAL treatment did, which may be indicative of less mature bone tissue that has not yet undergone remodeling to remove carbonate. Two studies have examined the response of osteoblastic cells to carbonated hydroxyapatite in comparison to pure hydroxyapatite (HA). When considered together, these studies demonstrate that osteoblasts produce more mineral and proliferate more rapidly when in contact with carbonated HA [21,42]. Therefore, RAL-induced bone formation on the periosteal surface may utilize increased carbonation to enhance the capacity for osteoblasts to lay new bone. In terms of mechanical properties, previous studies have demonstrated a negative correlation between carbonate substitution and fracture toughness on the whole bone level and reduced modulus and hardness on the tissue level [28,41]. Interestingly, no correlation was seen with structural mechanical properties including modulus and ultimate strength [9]. Decreased tissue-level properties are thought to be related to internal strains created by carbonate within the bone matrix that result in altered crystal formation and elongation [6]. In our study, we did not observe changes in reduced modulus or hardness in RAL-treated samples in regions with increased relative carbonate content. We hypothesize that RAL may interact with the matrix and stabilize mineral crystals that contain carbonate substitutions, normalizing the mechanical properties of the region, a process that may also involve increased matrix-bound water.

It was further observed that RAL increased the relative collagen maturity of newly formed bone tissue. This parameter, measured as the 1660 cm^{-1}/1690 cm^{-1} subpeak area ratios, likely represents changes in the secondary structure of collagen due to changes in content or shape driven by increased mineralization [17]. In general, proper collagen structure and

alignment is responsible for providing bone tissue with toughness and post-yield mechanical integrity [43]. Thus, given these direct changes in the secondary structure of collagen, fatigue and fracture toughness testing may better reflect the mechanical outcome of these changes as compared to the monotonic test to failure that was performed in this study. Future work involving dynamic mechanical analysis can provide information on how collagen and RAL treatment impact the viscoelastic properties of bone on the microscale.

As a limitation, we note that in order to cut and polish bone samples for Raman spectroscopy and nanoindentation, bones were embedded in Koldmount, a fast-curing methyl methacrylate (MMA) resin. This method of embedding was selected because it does not require the bone to be dehydrated and it cures rapidly. A previous study demonstrated that embedding bone in polymethylmethacrylate (PMMA) significantly altered the mineral/matrix ratio normalized to the CH_2 wag peak [48]. However, this process utilized a slow-curing method that involved dehydration and soaking the bone in xylenes before undergoing a 7-day infiltration with MMA. In this case, bone composition is altered by dehydration and matrix infiltration which could result in increased free radical release deep into the bone matrix during polymerization. While the effects of Koldmount embedding on bone Raman signatures and other matrix properties have not been directly studied, this method does not require dehydration or infiltration and likely preserves hydration of the bone tissue and limits free radical infiltration to the bone surface. Therefore, alterations in the CH_2 wag peak area are less likely to have been caused by the method of embedding and may reflect actual changes in the protein content of the bone matrix.

In summary, it was demonstrated that RAL and loading work together to improve bone size and architecture, especially within the cancellous region. In the cortical regions, there were some combination effects in the males, even at the microstructural-level which showed load-based changes in mineralization and RAL-based changes in the secondary collagen structure. In females, the large load-based effects in the cortical region obscured many effects of RAL, though some effects were still present. Future work will aim to explore the response of combined treatment in diseased tissue, which may provide a platform to observe even greater effects and potentially reverse the negative quality-based impacts of disease.

Acknowledgements

This work was supported by the National Institutes of Health [JMW: AR067221 and AR072609; JGD: DK121399]; the National Science Foundation [AGB: DGE1333468]; and IUPUI IPREP [ANP: GM109432]

References

1. Akkus O, Adar F and Schaffler MB. Age-related changes in physicochemical properties of mineral crystals are related to impaired mechanical function of cortical bone. Bone. 2004;34(3):443–453. Available doi 10.1016/j.bone.2003.11.003 [PubMed: 15003792]
2. Allen MR, Aref MW, Newman CL, Kadakia JR and Wallace JM. Raloxifene Neutralizes Bone Brittleness Induced by Anti-Remodeling Treatment and Increases Fatigue Life Through Non-Cell Mediated Mechanisms. Actualizaciones en Osteologia. 2016;12(3):169–179. Available
3. Allen MR, Hogan HA, Hobbs WA, Koivuniemi AS, Koivuniemi MC and Burr DB. Raloxifene Enhances Material-Level Mechanical Properties of Femoral Cortical and Trabecular Bone. Endocrinology. 2007;148(8):3908–3913. Available from 10.1210/en.2007-0275 doi 10.1210/en.2007-0275 [PubMed: 17478550]

4. Allen MR, Iwata K, Sato M and Burr DB. Raloxifene enhances vertebral mechanical properties independent of bone density. Bone. 2006;39(5):1130–1135. Available [PubMed: 16814622]
5. Aref M, Gallant MA, Organ JM, Wallace JM, Newman CL, Burr DB, Brown DM and Allen MR. In vivo reference point indentation reveals positive effects of raloxifene on mechanical properties following 6 months of treatment in skeletally mature beagle dogs. Bone. 2013;56(2):10.1016/j.bone.2013.1007.1009. Available from http://www.ncbi.nlm.nih.gov/pmc/articles/PMC3873633/ doi 10.1016/j.bone.2013.07.009
6. Bala Y, Farlay D and Boivin G. Bone mineralization: from tissue to crystal in normal and pathological contexts. Osteoporos Int. 2013;24(8):2153–2166. Available [PubMed: 23229470]
7. Berman AG, Clauser CA, Wunderlin C, Hammond MA and Wallace JM. Structural and mechanical improvements to bone are strain dependent with axial compression of the tibia in female C57BL/6 mice. PLoS One. 2015;10(6):e0130504. Available [PubMed: 26114891]
8. Berman AG, Hinton MJ and Wallace JM. Treadmill running and targeted tibial loading differentially improve bone mass in mice. Bone reports. 2019;10:100195. Available [PubMed: 30701187]
9. Bi X, Patil CA, Lynch CC, Pharr GM, Mahadevan-Jansen A and Nyman JS. Raman and mechanical properties correlate at whole bone-and tissue-levels in a genetic mouse model. J Biomech. 2011;44(2):297–303. Available [PubMed: 21035119]
10. Bivi N, Hu H, Chavali B, Chalmers MJ, Reutter CT, Durst GL, Riley A, Sato M, Allen MR and Burr DB. Structural features underlying raloxifene's biophysical interaction with bone matrix. Bioorg Med Chem. 2016;24(4):759–767. Available [PubMed: 26795112]
11. Brewer V, Meyer BM, Keele MS, Upton SJ and Hagan RD. Role of exercise in prevention of involutional bone loss. Med Sci Sports Exerc. 1983;15(6):445–449. Available from http://www.ncbi.nlm.nih.gov/pubmed/6656552 [PubMed: 6656552]
12. Cranney A, Guyatt G, Griffith L, Wells G, Tugwell P and Rosen C. IX: Summary of Meta-Analyses of Therapies for Postmenopausal Osteoporosis. Endocr Rev. 2002;23(4):570–578. Available from 10.1210/er.2001-9002 doi 10.1210/er.2001-9002 [PubMed: 12202472]
13. Dalen N and Olsson KE. Bone mineral content and physical activity. Acta Orthop Scand. 1974;45(2):170–174. Available from http://www.ncbi.nlm.nih.gov/pubmed/4406972 [PubMed: 4406972]
14. De Souza RL, Matsuura M, Eckstein F, Rawlinson SC, Lanyon LE and Pitsillides AA. Non-invasive axial loading of mouse tibiae increases cortical bone formation and modifies trabecular organization: a new model to study cortical and cancellous compartments in a single loaded element. Bone. 2005;37(6):810–818. Available [PubMed: 16198164]
15. Delmas PD, Bjarnason NH, Mitlak BH, Ravoux A-C, Shah AS, Huster WJ, Draper M and Christiansen C. Effects of raloxifene on bone mineral density, serum cholesterol concentrations, and uterine endometrium in postmenopausal women. N Engl J Med. 1997;337(23):1641–1647. Available [PubMed: 9385122]
16. Ettinger B, Black DM, Mitlak BH, Knickerbocker RK, Nickelsen T, Genant HK, Christiansen C, Delmas PD, Zanchetta JR and Stakkestad J. Reduction of vertebral fracture risk in postmenopausal women with osteoporosis treated with raloxifene: results from a 3-year randomized clinical trial. JAMA. 1999;282(7):637–645. Available [PubMed: 10517716]
17. Farlay D, Duclos ME, Gineyts E, Bertholon C, Viguet-Carrin S, Nallala J, Sockalingum GD, Bertrand D, Roger T, Hartmann DJ, Chapurlat R and Boivin G. The ratio 1660/1690 cm(−1) measured by infrared microspectroscopy is not specific of enzymatic collagen cross-links in bone tissue. PLoS One. 2011;6(12):e28736. Available doi 10.1371/journal.pone.0028736 [PubMed: 22194900]
18. Fritton JC, Myers ER, Wright TM and van der Meulen MCH. Loading induces site-specific increases in mineral content assessed by microcomputed tomography of the mouse tibia. Bone. 2005;36(6):1030–1038. Available from http://www.sciencedirect.com/science/article/pii/S8756328205000621 doi 10.1016/j.bone.2005.02.013 [PubMed: 15878316]
19. Fuchs RK, Bauer JJ and Snow CM. Jumping improves hip and lumbar spine bone mass in prepubescent children: a randomized controlled trial. J Bone Miner Res. 2001;16(1):148–156. Available from http://www.ncbi.nlm.nih.gov/pubmed/11149479 doi 10.1359/jbmr.2001.16.1.148 [PubMed: 11149479]

20. Gallant MA, Brown DM, Hammond M, Wallace JM, Du J, Deymier-Black AC, Almer JD, Stock SR, Allen MR and Burr DB. Bone cell-independent benefits of raloxifene on the skeleton: a novel mechanism for improving bone material properties. Bone. 2014;61:191–200. Available doi 10.1016/j.bone.2014.01.009 [PubMed: 24468719]
21. Germaini MM, Detsch R, Grunewald A, Magnaudeix A, Lalloue F, Boccaccini AR and Champion E. Osteoblast and osteoclast responses to A/B type carbonate-substituted hydroxyapatite ceramics for bone regeneration. Biomed Mater. 2017;12(3):035008. Available doi 10.1088/1748-605X/aa69c3 [PubMed: 28351999]
22. Gizzo S, Saccardi C, Patrelli TS, Berretta R, Capobianco G, Di Gangi S, Vacilotto A, Bertocco A, Noventa M and Ancona E. Update on raloxifene: mechanism of action, clinical efficacy, adverse effects, and contraindications. Obstet Gynecol Surv. 2013;68(6):467–481. Available [PubMed: 23942473]
23. Hammond MA, Berman AG, Pacheco-Costa R, Davis HM, Plotkin LI and Wallace JM. Removing or truncating connexin 43 in murine osteocytes alters cortical geometry, nanoscale morphology, and tissue mechanics in the tibia. Bone. 2016;88:85–91. Available from https://pubmed.ncbi.nlm.nih.gov/27113527 https://www.ncbi.nlm.nih.gov/pmc/articles/PMC4899203/ doi 10.1016/j.bone.2016.04.021 [PubMed: 27113527]
24. Hammond MA, Gallant MA, Burr DB and Wallace JM. Nanoscale changes in collagen are reflected in physical and mechanical properties of bone at the microscale in diabetic rats. Bone. 2014;60:26–32. Available from http://www.sciencedirect.com/science/article/pii/S8756328213004766 doi 10.1016/j.bone.2013.11.015 [PubMed: 24269519]
25. Hammond MA, Laine TJ, Berman AG and Wallace JM. Treadmill exercise improves fracture toughness and indentation modulus without altering the nanoscale morphology of collagen in mice. PLoS One. 2016;11(9):e0163273. Available [PubMed: 27655444]
26. Johnston CC Jr., Bjarnason NH, Cohen FJ, Shah A, Lindsay R, Mitlak BH, Huster W, Draper MW, Harper KD, Heath H 3rd, Gennari C, Christiansen C, Arnaud CD and Delmas PD. Long-term effects of raloxifene on bone mineral density, bone turnover, and serum lipid levels in early postmenopausal women: three-year data from 2 double-blind, randomized, placebo-controlled trials. Arch Intern Med. 2000;160(22):3444–3450. Available doi 10.1001/archinte.160.22.3444 [PubMed: 11112238]
27. Lynch ME, Main RP, Xu Q, Walsh DJ, Schaffler MB, Wright TM and van der Meulen MC. Cancellous bone adaptation to tibial compression is not sex dependent in growing mice. J Appl Physiol (1985). 2010;109(3):685–691. Available from http://www.ncbi.nlm.nih.gov/pubmed/20576844 doi 10.1152/japplphysiol.00210.2010 [PubMed: 20576844]
28. Makowski AJ, Granke M, Ayala OD, Uppuganti S, Mahadevan-Jansen A and Nyman JS. Applying full spectrum analysis to a Raman spectroscopic assessment of fracture toughness of human cortical bone. Applied spectroscopy. 2017;71(10):2385–2394. Available [PubMed: 28708001]
29. McElderry J-DP, Zhu P, Mroue KH, Xu J, Pavan B, Fang M, Zhao G, McNerny E, Kohn DH, Franceschi RT, Holl MMB, Tecklenburg MMJ, Ramamoorthy A and Morris MD. Crystallinity and compositional changes in carbonated apatites: Evidence from (31)P solid-state NMR, Raman, and AFM analysis. J Solid State Chem. 2013;206:10.1016/j.jssc.2013.1008.1011. Available from https://pubmed.ncbi.nlm.nih.gov/24273344 https://www.ncbi.nlm.nih.gov/pmc/articles/PMC3835554/ doi 10.1016/j.jssc.2013.08.011
30. Meakin LB, Sugiyama T, Galea GL, Browne WJ, Lanyon LE and Price JS. Male mice housed in groups engage in frequent fighting and show a lower response to additional bone loading than females or individually housed males that do not fight. Bone. 2013;54(1):113–117. Available from http://www.sciencedirect.com/science/article/pii/S875632821300046X doi 10.1016/j.bone.2013.01.029 [PubMed: 23356987]
31. Newman CL, Creecy A, Granke M, Nyman JS, Tian N, Hammond MA, Wallace JM, Brown DM, Chen N, Moe SM and Allen MR. Raloxifene improves skeletal properties in an animal model of cystic chronic kidney disease. Kidney Int. 2016;89(1):95–104. Available from https://pubmed.ncbi.nlm.nih.gov/26489025 https://www.ncbi.nlm.nih.gov/pmc/articles/PMC4840093/ doi 10.1038/ki.2015.315 [PubMed: 26489025]
32. Powell KM, Brown AP, Skaggs CG, Pulliam AN, Berman AG, Deosthale P, Plotkin LI, Allen MR, Williams DR and Wallace JM. 6′-Methoxy Raloxifene-analog enhances mouse bone properties

with reduced estrogen receptor binding. Bone Reports. 2020;12:100246. Available from http://www.sciencedirect.com/science/article/pii/S235218722030005X doi 10.1016/j.bonr.2020.100246 [PubMed: 32016137]

33. Powell KM, Skaggs C, Pulliam A, Berman A, Allen MR and Wallace JM. Zoledronate and Raloxifene combination therapy enhances material and mechanical properties of diseased mouse bone. Bone. 2019;127:199–206. Available from http://www.sciencedirect.com/science/article/pii/S8756328219302509 doi 10.1016/j.bone.2019.06.018 [PubMed: 31233931]
34. Sarkar S, Mitlak BH, Wong M, Stock JL, Black DM and Harper KD. Relationships between bone mineral density and incident vertebral fracture risk with raloxifene therapy. J Bone Miner Res. 2002;17(1):1–10. Available [PubMed: 11771654]
35. Sato ET and Martinho H. First-principles calculations of Raman vibrational modes in the fingerprint region for connective tissue. Biomed Opt Express. 2018;9(4):1728–1734. Available doi 10.1364/boe.9.001728 [PubMed: 29675314]
36. Seeman E, Crans GG, Diez-Perez A, Pinette KV and Delmas PD. Anti-vertebral fracture efficacy of raloxifene: a meta-analysis. Osteoporos Int. 2006;17(2):313–316. Available [PubMed: 16217588]
37. Sugiyama T, Price JS and Lanyon LE. Functional adaptation to mechanical loading in both cortical and cancellous bone is controlled locally and is confined to the loaded bones. Bone. 2010;46(2):314–321. Available from http://www.sciencedirect.com/science/article/pii/S8756328209018845 doi 10.1016/j.bone.2009.08.054 [PubMed: 19733269]
38. Sun D, Brodt MD, Zannit HM, Holguin N and Silva MJ. Evaluation of loading parameters for murine axial tibial loading: Stimulating cortical bone formation while reducing loading duration. Journal of Orthopaedic Research®. 2018;36(2):682–691. Available [PubMed: 28888055]
39. Taranta A, Brama M, Teti A, Scandurra R, Spera G, Agnusdei D, Termine J and Migliaccio S. The selective estrogen receptor modulator raloxifene regulates osteoclast and osteoblast activity in vitro. Bone. 2002;30(2):368–376. Available [PubMed: 11856644]
40. Tommasini SM, Nasser P and Jepsen KJ. Sexual dimorphism affects tibia size and shape but not tissue-level mechanical properties. Bone. 2007;40(2):498–505. Available from http://www.sciencedirect.com/science/article/pii/S8756328206006843 doi 10.1016/j.bone.2006.08.012 [PubMed: 17035111]
41. Unal M, Uppuganti S, Timur S, Mahadevan-Jansen A, Akkus O and Nyman JS. Assessing matrix quality by Raman spectroscopy helps predict fracture toughness of human cortical bone. Sci Rep. 2019;9(1):1–13. Available [PubMed: 30626917]
42. Uskokovic V, Janković-Častvan I and Wu V. Bone Mineral Crystallinity Governs the Orchestration of Ossification and Resorption during Bone Remodeling. ACS Biomaterials Science & Engineering. 2019;5. Available doi 10.1021/acsbiomaterials.9b00255
43. Wang X, Shen X, Li X and Agrawal CM. Age-related changes in the collagen network and toughness of bone. Bone. 2002;31(1):1–7. Available doi 10.1016/s8756-3282(01)00697-4 [PubMed: 12110404]
44. Weatherholt AM, Fuchs RK and Warden SJ. Cortical and trabecular bone adaptation to incremental load magnitudes using the mouse tibial axial compression loading model. Bone. 2013;52(1):372–379. Available [PubMed: 23111313]
45. Willie BM, Birkhold AI, Razi H, Thiele T, Aido M, Kruck B, Schill A, Checa S, Main RP and Duda GN. Diminished response to in vivo mechanical loading in trabecular and not cortical bone in adulthood of female C57Bl/6 mice coincides with a reduction in deformation to load. Bone. 2013;55(2):335–346. Available from http://www.ncbi.nlm.nih.gov/pubmed/23643681 doi 10.1016/j.bone.2013.04.023 [PubMed: 23643681]
46. Wolman RL, Faulmann L, Clark P, Hesp R and Harries MG. Different training patterns and bone mineral density of the femoral shaft in elite, female athletes. Ann Rheum Dis. 1991;50(7):487–489. Available from http://www.ncbi.nlm.nih.gov/pubmed/1877854 [PubMed: 1877854]
47. Yang H, Embry RE and Main RP. Effects of loading duration and short rest insertion on cancellous and cortical bone adaptation in the mouse tibia. PLoS One. 2017;12(1):e0169519. Available [PubMed: 28076363]

48. Yeni YN, Yerramshetty J, Akkus O, Pechey C and Les CM. Effect of fixation and embedding on Raman spectroscopic analysis of bone tissue. Calcif Tissue Int. 2006;78(6):363–371. Available doi 10.1007/s00223-005-0301-7 [PubMed: 16830201]

49. Yerramshetty JS, Lind C and Akkus O. The compositional and physicochemical homogeneity of male femoral cortex increases after the sixth decade. Bone. 2006;39(6):1236–1243. Available doi 10.1016/j.bone.2006.06.002 [PubMed: 16860007]

50. Zapanta-LeGeros R Effect of carbonate on the lattice parameters of apatite. Nature. 1965;206(982):403–404. Available doi 10.1038/206403a0 [PubMed: 5835710]

51. Zhao C, Hou H, Chen Y and Lv K. Effect of aerobic exercise and raloxifene combination therapy on senile osteoporosis. Journal of physical therapy science. 2016;28(6):1791–1794. Available [PubMed: 27390417]

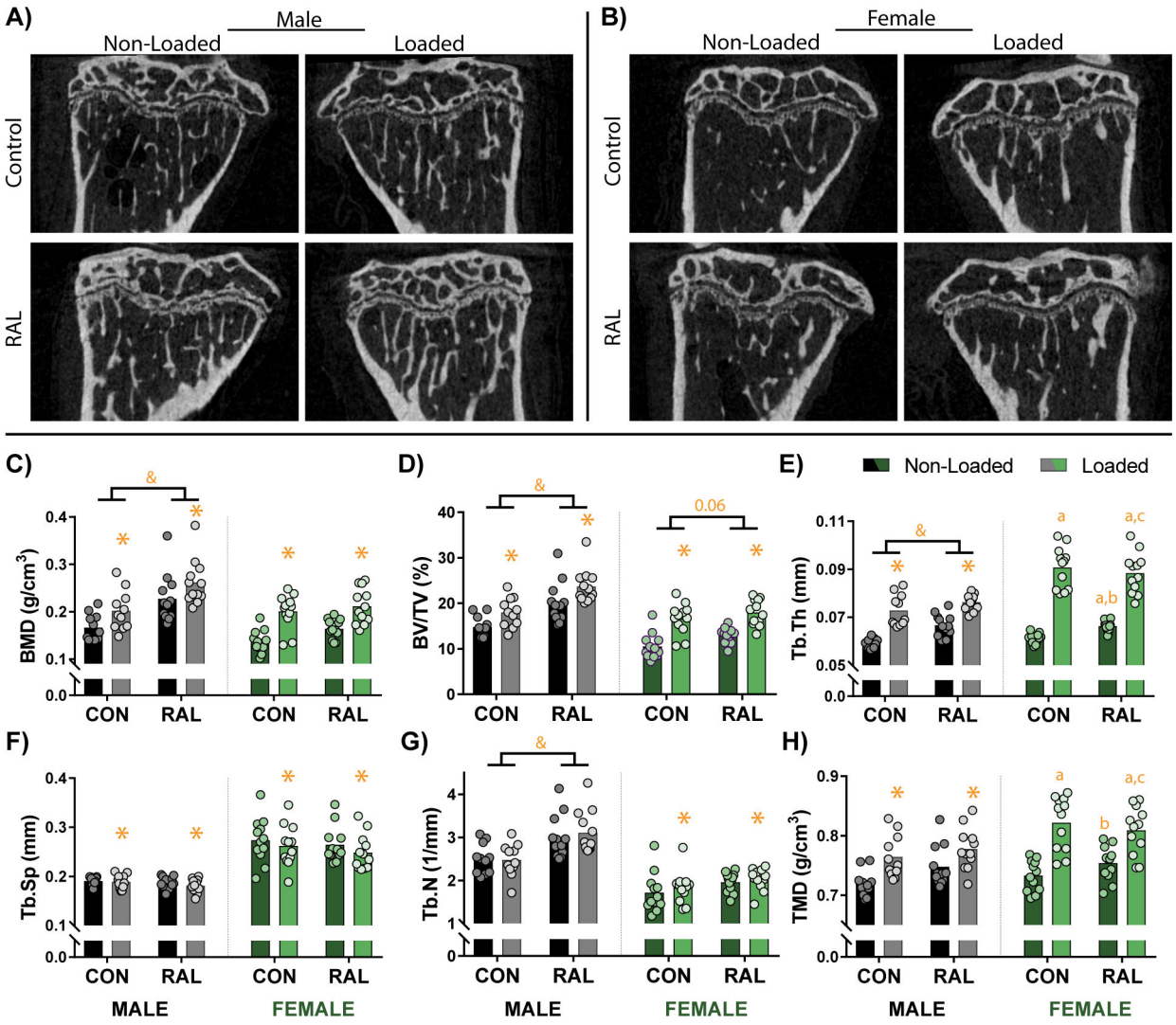

Figure 1.

Sagittal CT images of the proximal tibia from (**A)** male and (**B)** female mice qualitatively show increased cancellous bone due to loading and RAL. (**C)** Quantitative measures of bone mineral density (BMD) and (**D)** bone volume fraction (BV/TV) similarly indicate additive mass-based effects due to loading and RAL in males. In females, the loading had the more prominent effect than RAL. (**E)** These improvements were driven by load- and RAL-based increases to trabecular thickness (Tb.Th), (**F)** load-based decreases to trabecular spacing (Tb.Sp), and (**G)** load- and RAL-based increases in trabecular number (Tb.N). (**H)** In addition, tissue mineral density (TMD) was increased due to loading in both males and females. For a two-way ANOVA, a '&' indicates a main effect of RAL and an '*' indicates a main effect of loading. If the interaction term was significant, an 'a' indicates a significant difference from non-loaded control, 'b' indicates a significant difference from loaded control, and 'c' indicates a significant difference from non-loaded RAL.

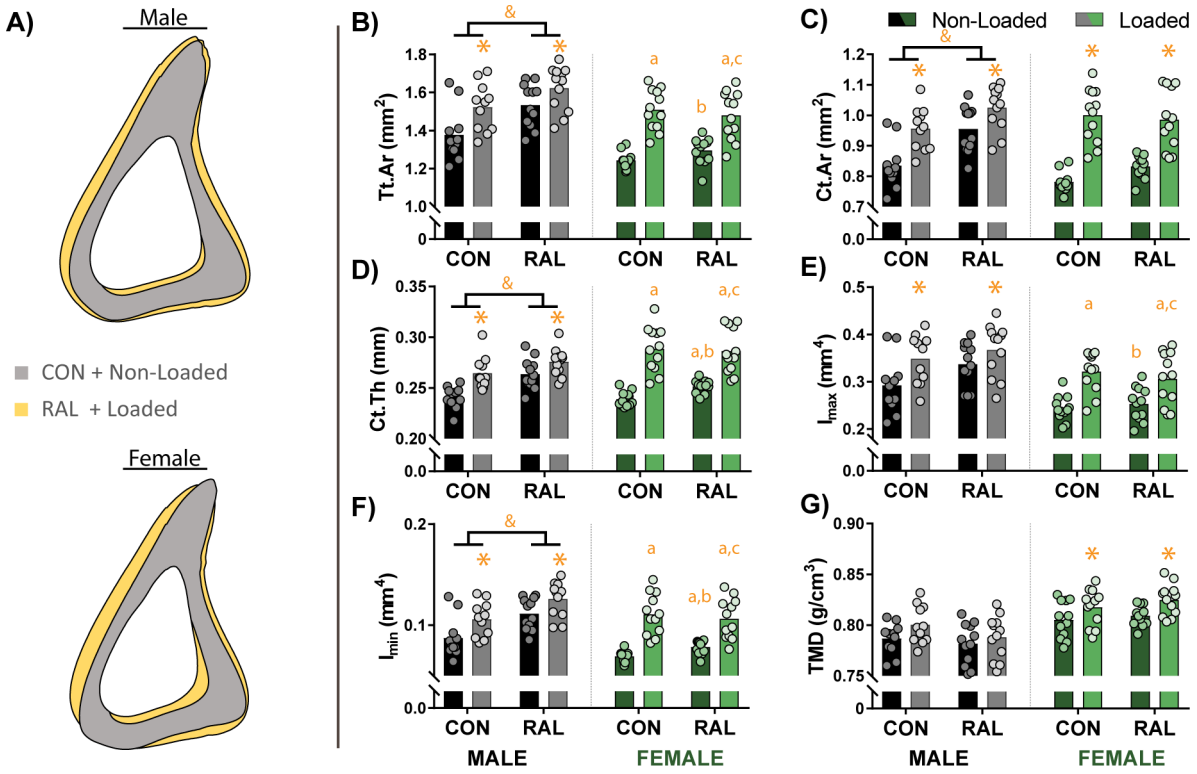

Figure 2.

(**A)** Averaged cortical profiles of male and female mice at the proximal-mid position show improvements due to loading and RAL. (**B)** Measures of the total cross-sectional area (Tt.Ar), (**C)** cortical area (Ct.Ar), and (**D)** cortical thickness (Ct.Th) were significantly impacted by both load and RAL in males, resulting in a graded response. In contrast, in females, while there was some effects of RAL, the robust increases were primarily driven by load. (**E)** Maximum moment of inertia (I_{max}) was impacted by loading in both sexes, while (**F)** minimum moment of inertia (I_{min}) was positively influenced by RAL as well as the loading. (**G)** Tissue mineral density (TMD) showed no response in males, while it was significantly increased with loading in females. For a two-way ANOVA, a '&' indicates a main effect of RAL and an '*' indicates a main effect of loading. If the interaction term was significant, an 'a' indicates a significant difference from non-loaded control, 'b' indicates a significant difference from loaded control, and 'c' indicates a significant difference from non-loaded RAL.

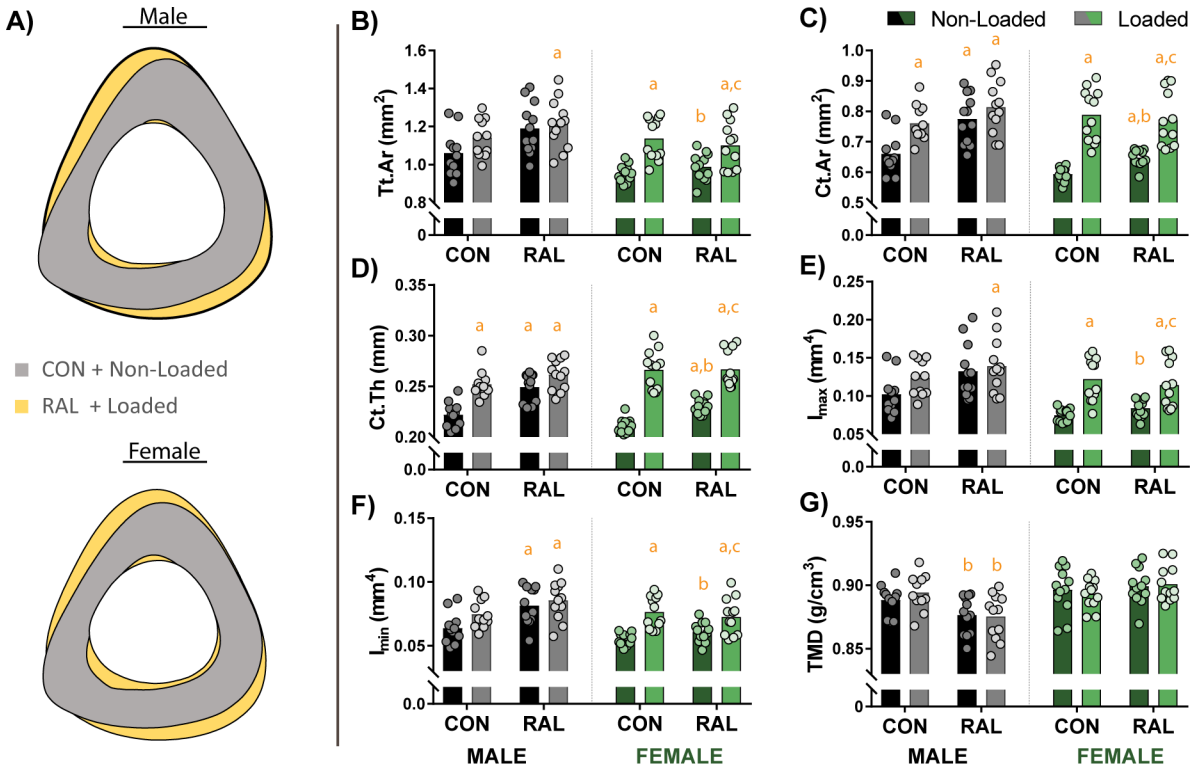

Figure 3.

(**A)** Averaged cortical profiles of male and female mice at the mid location show large improvements due to loading (both males and females) and RAL (primarily males). (**B)** Measures of total cross-sectional area (Tt.Ar) indicate a graded response in males, only reaching significance in the combined treatment. In contrast, in females, the robust increases in CSA were driven by load. (**C)** Cortical area (Ct.Ar) and (**D)** cortical thickness (Ct.Th) were increased due to both load and RAL. However, the load-response was more robust than the RAL response in females. (**E)** Maximum and (**F)** minimum moments of inertia were both increased due to loading and RAL in both sexes. (**G)** Tissue mineral density (TMD) showed very little effects. For a two-way ANOVA, a '&' indicates a main effect of RAL and an '*' indicates a main effect of loading. If the interaction term was significant, an 'a' indicates a significant difference from non-loaded control, 'b' indicates a significant difference from loaded control, and 'c' indicates a significant difference from non-loaded RAL.

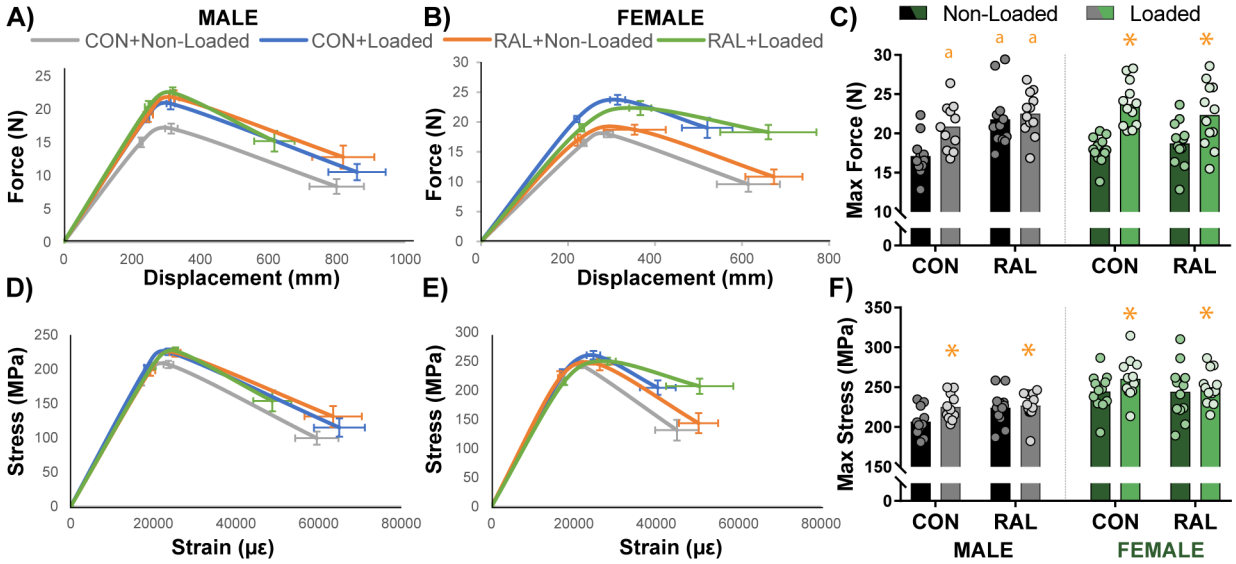

Figure 4.

(**A)** Averaged force-displacement plots for male mice show an upward shift in the strength of tibiae that received loading, RAL, and both. (**B)** In female mice, improvements in mechanical properties was primarily driven by loading, as can be observed in (**C)** maximum force. After normalizing to cross-sectional area, stress-strain plots for (**D)** male and (**E)** female showed similar results as the force-displacement plots, as can also be observed in (**F)** maximum stress. Plots are shown as average ± SEM. For a two-way ANOVA, a '&' indicates a main effect of RAL and an '*' indicates a main effect of loading. If the interaction term was significant, an 'a' indicates a significant difference from non-loaded control, 'b' indicates a significant difference from loaded control, and 'c' indicates a significant difference from non-loaded RAL.

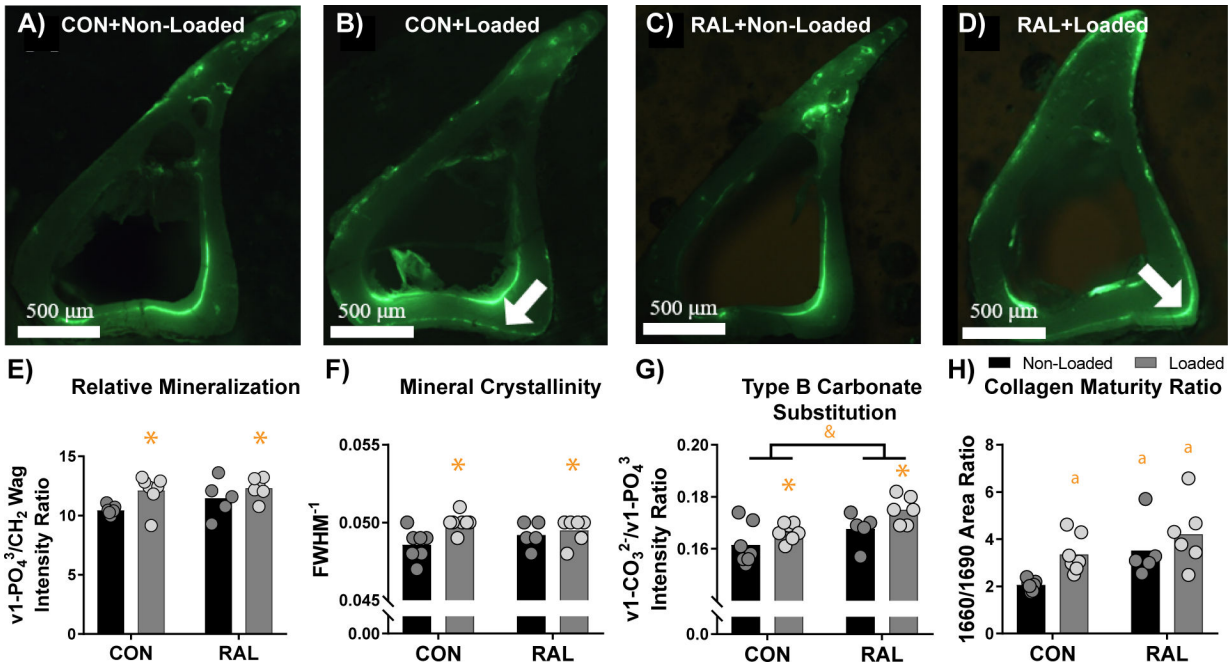

Figure 5.

Raman spectra of newly formed bone were acquired in (**A)** non-loaded control, (**B)** loaded control, (**C)** non-loaded RAL, and (**D)** loaded RAL tibiae using fluorescent calcein labelling for visualization. White arrows show regions of periosteal bone growth in the loaded limbs. (**E)** Relative mineralization and (**F)** mineral crystallinity were both elevated due to loading, while (**G)** Type B carbonate substitution was increased due to RAL. (**H)** Collagen maturity ratio indicated increased collagen maturity due to both loading and RAL. For a two-way ANOVA, a '&' indicates a main effect of RAL and an '*' indicates a main effect of loading. If the interaction term was significant, an 'a' indicates a significant difference from non-loaded control, 'b' indicates a significant difference from loaded control, and 'c' indicates a significant difference from non-loaded RAL. Arrows indicate locations of new bone growth.

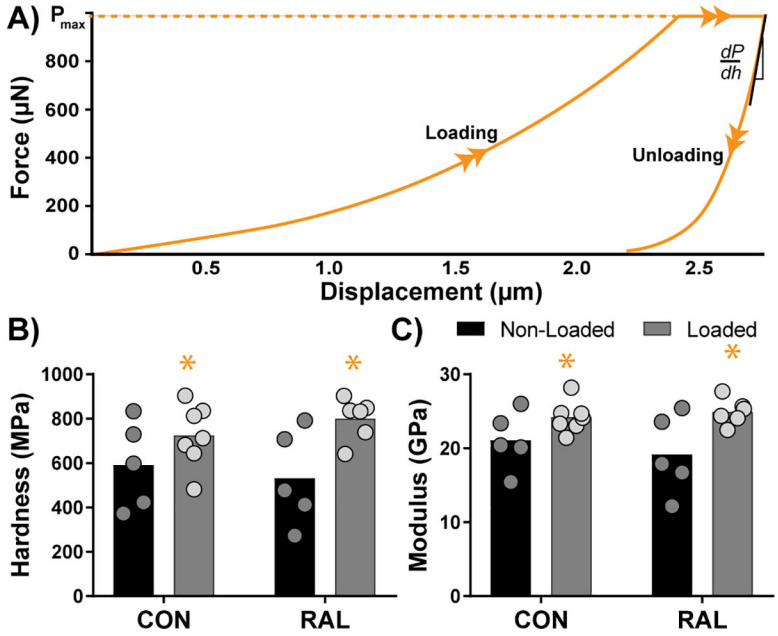

Figure 6.

(**A)** Representative indentation plot showing loading and unloading curves. (**B)** Hardness and (**C)** modulus both showed increases due to loading, but not due to RAL.

Table 1.

Number of mice used for each cohort. For each mouse, both right and left tibiae were analyzed (loaded versus non-loaded).

	COHORT 1		COHORT 2		TOTAL
	CON	RAL	CON	RAL	
MALE	11	12	8	8	39
FEMALE	12	12	N/A	N/A	24

Table 2.

Mechanical properties for male and female mice.

	CON	LOAD	RAL	RAL+LOAD
MALE	**(n=11)**	**(n=11)**	**(n=12)**	**(n=12)**
Yield Force (N) *+	15.0±2.5	18.8±2.5	18.3±1.9	20.1±3.0
Maximum Force (N)	17.1±2.6	20.9±3.0[a]	21.8±3.7[a]	22.5±2.8[a]
Displacement to Yield (μm)	227±17	250±16[a]	233±5	238±14
Postyield Displacement (μm)	572±260	616±294	571±324	369±206
Total Displacement (μm)	799±265	859±278	819±315	617±205
Stiffness (N/mm) *	75.4±13.1	89.3±23.7	86.3±11.5	92.2±12.8
Work to Yield (mJ)	1.87±0.32	2.48±0.27[a]	2.34±0.24[a]	2.51±0.28[a]
Postyield Work (mJ)	6.12±2.81	9.17±5.64	8.21±3.84	6.35±3.34
Total Work (mJ)	7.99±2.71	11.64±5.56	10.83±3.88	9.12±3.45
Yield Stress (MPa) *	181±18	203±10	198±27	204±17
Maximum Stress (MPa) *	207±18	225±17	224±21	227±17
Strain to Yield (mε)	17.1±1.4	18.4±2.0	18.1±0.6	18.8±0.6
Total Strain (mε)	59.5±18.2	65.0±21.4	63.5±24.0	48.8±16.0
Modulus (GPa)	12.0±0.8	12.7±2.2	11.8±2.1	12.0±0.9
Resilience (MPa) *	1.71±0.27	2.03±0.19	1.94±0.15	2.06±0.19
Toughness (MPa)	7.39±2.72	9.44±3.92	8.73±3.11	7.34±2.93
FEMALE	**(n=12)**	**(n=12)**	**(n=12)**	**(n=12)**
Yield Force (N) *	16.5±1.9	20.5±1.9	17.0±3.3	19.0±2.1
Maximum Force (N) *	17.9±1.7	23.7±2.9	18.7±2.9	22.3±4.1
Displacement to Yield (μm)	237±18	220±20	222±21	231±18
Postyield Displacement (μm)	378±252	300±205	451±232	429±373
Total Displacement (μm)	615±251	520±201	673±227	661±383
Stiffness (N/mm)	79.3±11.9	107.3±19.9 [a]	87.9±21.2 [b]	93.5±12.3
Work to Yield (mJ) *	2.14±0.27	2.46±0.17	2.07±0.38	2.41±0.32
Postyield Work (mJ)	4.13±2.22	6.06±4.60	6.13±3.32	8.30±6.78
Total Work (mJ)	6.27±2.09	8.53±4.62	8.20±3.23	10.71±6.94
Yield Stress (MPa)	225±29	227±33	221±40	215±22
Maximum Stress (MPa) *	245±23	260±26	244±34	250±21
Strain to Yield (mε)	17.3±1.4	17.2±1.3	16.6±1.5	17.7±1.1
Total Strain (mε)	45.0±18.3	40.4±14.9	50.3±16.5	50.5±28.3
Modulus (GPa)	14.8±2.4	15.1±3.3	15.3±3.2	13.8±1.5
Resilience (MPa)	2.14±0.28	2.13±0.25	2.02±0.38	2.09±0.28
Toughness (MPa)	6.25±1.99	7.41±3.99	7.96±3.15	8.92±5.32

A '*' indicates a significant effect of load and a '+' indicates a significant effect of treatment ($p<0.05$).In the case of significant interaction term, a one-way ANOVA with post-hoc Tukey HSD test was performed.

An ‘a’ indicates a significant difference from CON, a ‘b’ indicates a significant difference from LOAD, and a ‘c’ indicates a significant difference from RAL ($p<0.05$).